RSC Medicinal Chemistry

ROYAL SOCIETY OF CHEMISTRY

RESEARCH ARTICLE

View Article Online
View Journal | View Issue

Cite this: *RSC Med. Chem.*, 2024, **15**, 3746

Novel PROTAC probes targeting KDM3 degradation to eliminate colorectal cancer stem cells through inhibition of Wnt/β-catenin signaling†

Shadid U. Zaman,‡[a] Piyusha P. Pagare,‡[a] Hongguang Ma,[a] Rosalie G. Hoyle,[a] Yan Zhang *[a] and Jiong Li *[abc]

Received 20th February 2024,
Accepted 20th August 2024

DOI: 10.1039/d4md00122b

rsc.li/medchem

It has been demonstrated that the KDM3 family of histone demethylases (KDM3A and KDM3B) epigenetically control the functional properties of colorectal cancer stem cells (CSCs) through Wnt/β-catenin signaling. Meanwhile, a broad-spectrum histone demethylase inhibitor, IOX1, suppresses Wnt-induced colorectal tumorigenesis predominantly through inhibiting the enzymatic activity of KDM3. In this work, several cereblon (CRBN)-recruiting PROTACs with various linker lengths were designed and synthesized using IOX1 as a warhead to target KDM3 proteins for degradation. Two of the synthesized PROTACs demonstrated favorable degradation profile and selectivity towards KDM3A and KDM3B. Compound **4** demonstrated favorable *in vitro* metabolic profile in liver enzymes as well as no hERG-associated cardiotoxicity. Compound **4** also showed dramatic ability in suppressing oncogenic Wnt signaling to eliminate colorectal CSCs and inhibit tumor growth, with around 10- to 35-fold increased potency over IOX1. In summary, this study suggests that PROTACs provide a unique molecular tool for the development of novel small molecules from the IOX1 skeleton for selective degradation of KDM3 to eliminate colorectal CSCs *via* suppressing oncogenic Wnt signaling.

Introduction

Colorectal cancer (CRC) is the third most commonly diagnosed type of cancer and second leading cause of cancer-related deaths worldwide with about 935 000 deaths reported in 2020.[1] An increase in early detection has significantly improved the overall survival rate in CRC to 64%, but the 5 year survival rate for stage IV (metastatic) CRC remains unimproved at around 12% due to the lack of effective treatment options.[1,2] Over 90% of all CRC cases are associated with hyperactivation of Wnt/β-catenin signaling, and Wnt/β-catenin signaling has been demonstrated to play an essential role in sustaining tumor CRC growth and development.[3–7] Meanwhile, high Wnt activity has been shown to be a vital characteristic and a key driver of human colorectal cancer stem cells (CSCs) which are responsible for tumorigenesis, metastasis, and development of chemotherapy resistance. In fact, major functional markers of colorectal CSCs such as *LGR5*, *ZNRF3*, *RNF43* and *ASCL2* are Wnt direct target genes.[7–12] The significance of Wnt signaling in CRC initiation and development, and validation of the Wnt signaling as a therapeutic target for CRC have already been well-recognized.[13,14] Although substantial effort has been invested in therapeutically inhibiting Wnt/β-catenin signaling, no drug has reached clinics, indicating the urgent need for identifying new drug targets and developing more effective strategies to suppress oncogenic Wnt signaling.

Our group has previously demonstrated that a KDM3 family of histone demethylases, specifically KDM3A and KDM3B, are significantly upregulated in colorectal CSCs and maintain the tumorigenic potential of colorectal CSCs through Wnt/β-catenin signaling. We also demonstrated that IOX1, a broad-spectrum inhibitor of histone demethylases, including KDM3, KDM4, KDM6B, and KDM2A, significantly suppresses Wnt/β-catenin signaling and the functional properties of colorectal CSCs primarily through inhibiting the enzymatic activity of KDM3.[15,16] We showed that colorectal CSCs are more sensitive to IOX1 than non-CSCs,

[a] *Department of Medicinal Chemistry, School of Pharmacy, Virginia Commonwealth University, Richmond, Virginia 23298-0540, USA. E-mail: yzhang2@vcu.edu, jli29@vcu.edu*
[b] *Department of Oral and Craniofacial Molecular Biology, Virginia Commonwealth University, Richmond, Virginia 23298-0540, USA*
[c] *Massey Cancer Center, Virginia Commonwealth University, Richmond, Virginia 23298-0540, USA*

† Electronic supplementary information (ESI) available. See DOI: https://doi.org/10.1039/d4md00122b

‡ These authors contributed equally.

which makes IOX1 a promising structure to be optimized to develop new molecules that selectively target CSCs. However, IOX1 lacks selectivity between KDM3 and KDM4 family members and its potency for suppressing CRC tumorigenesis is relatively low with effective concentrations for suppressing CSC growth being 20–50 μM in most cell-based assays.[16,17]

In this work, we demonstrated that the shortcomings of IOX1 can be overcome by designing proteolysis targeting chimeras (PROTACs) carrying various linker lengths with the aim of improving selectivity and potency towards KDM3. PROTACs are being extensively studied as anti-cancer therapeutics.[18,19] PROTACs can afford an advantage over the parent compound, IOX1, because they are expected to work catalytically to facilitate proteasomal degradation and thereby improve potency.[20] Furthermore, it has been demonstrated that the linker length between the warhead and the E3 ligand can affect the selectivity towards the target protein.[21–23] Thus, a series of PROTACs were synthesized utilizing IOX1 as the warhead and pomalidomide as the (cereblon-recruiting) E3 ligand, and their selectivity towards KDM3 and efficacy in suppressing CRC tumorigenesis were evaluated using *in vitro* and *in vivo* CRC models. We identified two potent IOX1-based PROTACs which selectively degraded KDM3 by optimizing the linker length, demonstrating the feasibility of improving the potency and selectivity toward KDM3 from the IOX1 skeleton *via* PROTAC modifications. Our study provides the proof-of-concept evidence that optimization of IOX1-based PROTACs creates opportunities for the selective degradation of KDM3 proteins, thereby effectively eliminating colorectal CSCs through inhibition of Wnt signaling, which can be tailored to develop novel Wnt-dependent targeted therapies to treat CRC.

Results and discussion

Molecular design and synthesis

A successful PROTAC is designed such that it brings together the protein of interest and E3-ligase to facilitate the ubiquitination of the protein of interest *via* the E3-ligase.[18,24,25] Thus, the linker length, orientation, and point of attachment play an important role in its design. A structure-based approach was utilized to rationalize the molecular design of IOX1-based PROTACs. Employing molecular docking studies, previously it was demonstrated that IOX1 showed identical interactions with both KDM3A and KDM3B, and hence, in our current work we focused on the KDM3B–IOX1 protein–ligand complex.[16] Our docking results showed that the hydroxy group was positioned to direct a linker chain towards the solvent-exposed area upon attachment. However, we recognized that the resulting phenolic esters would be suboptimal due to their chemical instability. Conversely, the carboxy group of IOX1, although bound within the binding pocket, was situated such that an ester or amide linkage would guide the linker chain out of the pocket and towards the solvent-exposed area (Fig. 1 and Hoyle 2021 (ref. 16). Thus, this carboxy group was defined as the point of attachment for the linker in our PROTAC design.

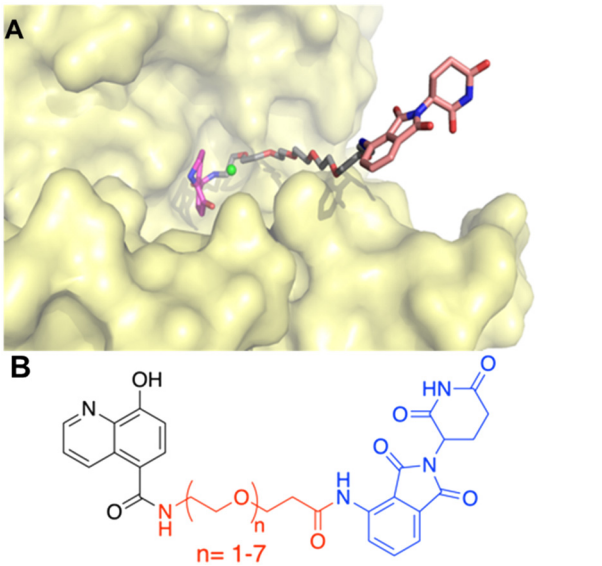

Fig. 1 (A) Binding pose of the optimal IOX1-PEG-polidomide (E3-ligand) in KDM3B (IOX1: magenta, PEG-linker: grey, pomalidomide: pink sticks, metal ion (Mn): green sphere, KDM3B: yellow surface; (B) chemical structure of synthesized PROTAC probes (IOX1: black, PEG-linker: red, pomalidomide: blue).

As mentioned above, the optimal linker would facilitate the ubiquitination of the target protein, KDM3B, but not too long or too short to compromise the degradation efficiency.[21,26–28] Polyethylene glycols (PEGs) with different chain lengths are the most commonly used PROTAC linkers accounting for almost 55% among published PROTAC molecules.[28–30] Due to this and their commercial availability, PEG was chosen as the linker type. To determine the optimal linker length, IOX1 derivatives with various lengths of PEG chains were docked in the binding pocket of KDM3B (PDB ID: 4C8D) using GOLD2020.[31,32] Following energy minimization of the highest scored protein–ligand complexes, it was observed that a minimum of 14-atoms were required for the linker to be out of the binding pocket of KDM3B and in the solvent exposed region (Fig. 1A). In addition, analyzing the X-ray structures of PROTAC bound ternary complexes of the CRBN-E3-ligase revealed that at least 4-atoms were required for the linker to be outside the binding pocket in the solvent exposed region from the E3-ligase.[33] Thus, taken together along with the orientation of the KDM3B target protein, the starting point for exploring the linker length was determined to be 17 atoms (Fig. 1B). The flexible nature of PEG linkers makes it challenging to predict the optimal binding pose reliably using binary molecular docking studies. Nevertheless, molecular docking results were utilized to establish a reasonable starting point for exploring linker lengths. In order to

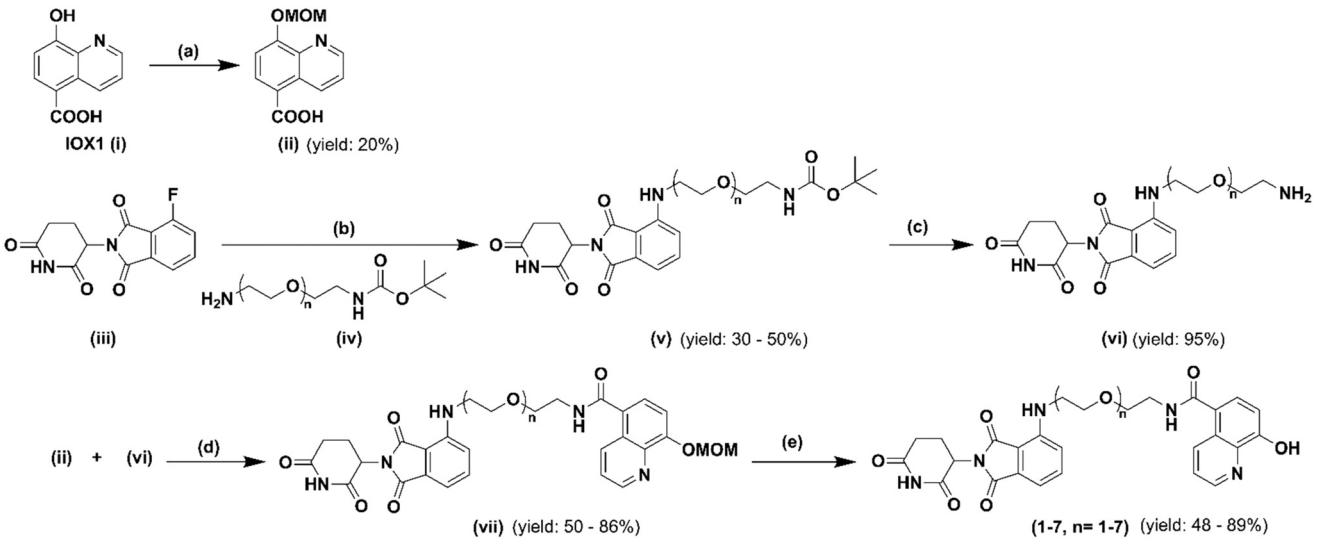

Scheme 1 Synthetic route for IOX1 PROTAC analogs: (a) MOM-Br, NAH, LiOH, THF, 0 °C; (b) DMA, DIPEA, 90 °C; (c) TFA, DCM, rt; (d) EDCI, HOBt, DMF, rt; (e) HCl, 1,4-dioxane, rt.

calibrate the optimal linker length, PEG linkers with chain lengths 6 (PEG n = 1) – 24 (PEG n = 7) were explored. Lastly, thalidomide and its derivatives are one of the most reported CRBN selective E3-ligase ligands utilized for PROTACs including ARV-110 and ARV-471.[33–39] Hence, thalidomide was selected as the E3-ligase ligand for PROTAC synthesis. Overall, this exploratory molecular design resulted in seven IOX1-based PROTAC analogs.

The synthetic route of the newly designed compounds **1**–**7** is outlined in Scheme 1. First, protection of the hydroxyl group on IOX1 was furnished by converting it to its methoxymethyl (MOM) ether. Second, pomalidomide, a derivative of thalidomide, was coupled with commercially available *tert*-butyloxycarbonyl protected polyethylene glycol (PEG) linkers of various lengths. After treatment with trifluoracetic acid to obtain the free amine, MOM-protected IOX1 and the linker–E3 ligase complex were coupled *via* the EDCI/HOBt coupling reaction. Finally, the hydroxyl group on IOX1 was deprotected under acidic conditions and the compounds were converted to their hydrochloride salt forms, fully characterized and submitted for subsequent *in vitro* and *in vivo* biological studies.

Wnt luciferase report assay

To identify the most potent compounds in suppressing Wnt signaling effectively, we adopted our well-established Wnt luciferase reporter assays to assess their inhibitory activity in the 293T cells expressing a TCF-responsive luciferase reporter (293T-TCF-Luc).[15] The cells were pre-treated with IOX1 or its respective PROTAC (compounds **1**–**7**) for 4 hours, followed by 12 hour treatment of 20 mM LiCl, a GSK3 inhibitor, which induces the β-catenin/TCF-mediated transcription. Inhibition of the β-catenin-dependent transcription by the assayed compounds reduced expression of the luciferase activity which is indicated by reduction in luminescence. IOX1 and the seven PROTACs all showed dose-dependent reduction in luciferase activity upon 16 hour treatment but the PROTACs demonstrated lower IC_{50} values compared to the parent compound (Fig. 2A). Compound **4** was the most potent with

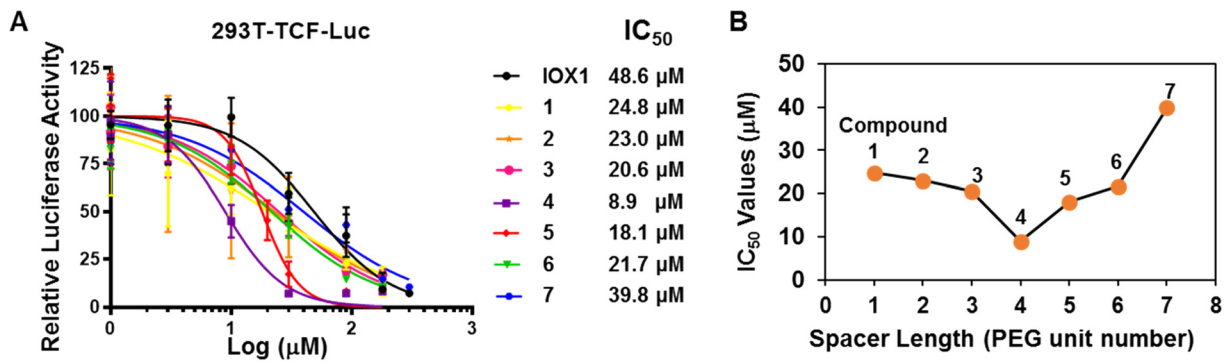

Fig. 2 IOX1-PROTACs potently suppress Wnt signaling in CRC cells. (A) IOX1-PROTACs inhibited the Wnt luciferase reporter in 293T cells. (B) The relationship of the linker length with the IC_{50} of the IOX1-PROTACs.

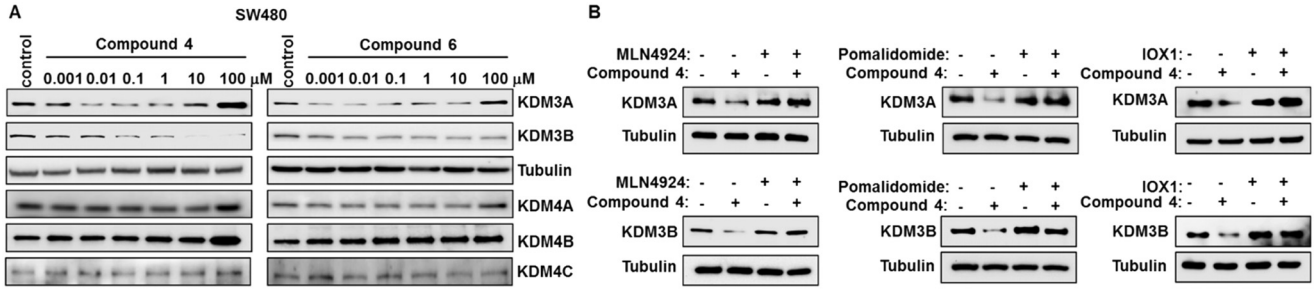

Fig. 3 IOX1-PROTACs induced KDM3A and KDM3B degradation in SW480 cells. (A) SW480 cells were treated with compounds **4** or **6** as indicated for 16 hours. (B) MLN4924, pomalidomide, or IOX1 restored PROTAC-induced KDM3A/B degradation in SW480 cells. MLN4924: 1 μM; pomalidomide: 100 μM; compound **4**: 0.1 μM for KDM3A western blot and 1 μM for KDM3B western blot.

a five-fold lower IC_{50} compared to IOX1 (8.9 μM *vs.* 48.6 μM, respectively). Furthermore, a clear relationship was observed between the IC_{50} and the spacer length between the warhead and the E3 ligand components of the PROTACs, with the linker length of 4 PEG units being the most optimal for activity (Fig. 2B). This corresponds to a linker length of 16 atoms which is very close to our proposed design. Our finding suggests that there is a "sweet-spot" of linker length for activity, a shorter linker length is insufficient, while a linker length longer than that also reduces activity.

Degradation profiles of IOX1 PROTACs

Since IOX1 can inhibit both KDM3 (KDM3A and KDM3B) and KDM4 (KDM4A, KDM4B and KDM4C) families of histone demethylases, the IOX1-based PROTACs may degrade both KDM3 and KDM4 proteins.[17] Based on the IC_{50} values obtained from the luciferase assay, compounds **3**, **4**, **5** and **6** were chosen for evaluation of the protein degradation profile in human CRC SW480 cells. Western blot analysis showed that compound **4** degrades both KDM3A and KDM3B at nanomolar concentrations, whereas compound **6** only has limited ability to degrade KDM3A and KDM3B in SW480 cells (Fig. 3A). In comparison, the parental compound, IOX1, did not induce KDM3A and KDM3B degradation in SW480 cells (Fig. S1†). Of note, the DC_{50} values of compound **4** are 13.73 nM and 172.6 nM for KDM3A and KDMB in SW480 cells, respectively (Fig. S2†). The D_{max} values of compound **4** are 65.34% and 88.55% for KDM3A and KDM3B, respectively. Compounds **3** and **5** had little effect in degrading KDM3A and KDM3B (data not shown). A "hook effect" was observed with compounds **4** and **6** for KDM3A degradation at higher doses in SW480 cells. The "hook effect" is an intrinsic property of any PROTAC.[40,41] This effect is a result of a saturation of PROTAC molecules that leads to increased binary complex formation and decreased ternary complex formation necessary for degradation and is correlated with the binding affinity of the warhead to the protein of interest. Since IOX1 has stronger binding affinity for KDM3A compared to other KDM proteins, this may explain why the "hook effect" is only observed for KDM3A degradation under the treatment conditions.[17,42] It was also noted that KDM4 family proteins were not dramatically affected by the PROTACs (compounds **4** and **6**). The KDM3 proteins' degradation profile was also evaluated in freshly isolated human CRC HCP-1 cells. As shown in Fig. S3,† compound **4** can also potently induce KDM3A and KDM3B degradation in HCP-1 cells. To validate the mechanism of action of PROTAC-induced degradation, a specific NEDD8-activating enzyme inhibitor, MLN4924, was adopted. As shown in Fig. 3B, the degradation of KDM3A or KDM3B induced by compound **4** could be restored by MLN4924 in SW480 cells. Furthermore, the degradation of KDM3A or KDM3B could also be suppressed by either pomalidomide or IOX1 in SW480 cells (Fig. 3B). Of note, pomalidomide treatment alone did not affect KDM3A or KDM3B expression in SW480 cells (Fig. S4A†). Finally, compounds **4** did not induce the known neo-substrate GSPT1 degradation in SW480 cells, which further confirmed the PROTAC-induced proteasomal degradation (Fig. S4B†). Taken together, our results indicated that the selectivity for KDM3 of the PROTAC molecules derived from the IOX1 can be achieved.

RT-qPCR analysis of Wnt target gene expression

Based on the degradation profile of compounds **4** and **6**, these were selected for further evaluation of the impact of KDM3 degradation on the Wnt signaling pathway. First, the basal toxicity of these two PROTACs was measured by CCK8 assay using non-malignant human colon epithelial cells, CRL-1790. Of note, KDM3 expression is undetected in CRL-1790. Both compounds had little impact on the cell growth in this cell line with TD_{50} values of 285.4 μM and 400.3 μM, respectively. (Fig. 4A). The cell growth was not dramatically affected at 60 μM for a two-day treatment. Therefore, concentrations below 60 μM were used for the following *in vitro* functional assays.

To determine the impact on Wnt target gene transcription, RNA extracts obtained from SW480 and HCP-1 following 16-hour treatment with IOX1, **4** or **6** were subjected to RT-qPCR. The two PROTACs were able to profoundly suppress expression of Wnt target genes, including *AXIN2*, *DKK1* and *CCND1*, by 50% or more in most cases at 50 μM concentration (Fig. 4B and S5†). The expression of colorectal

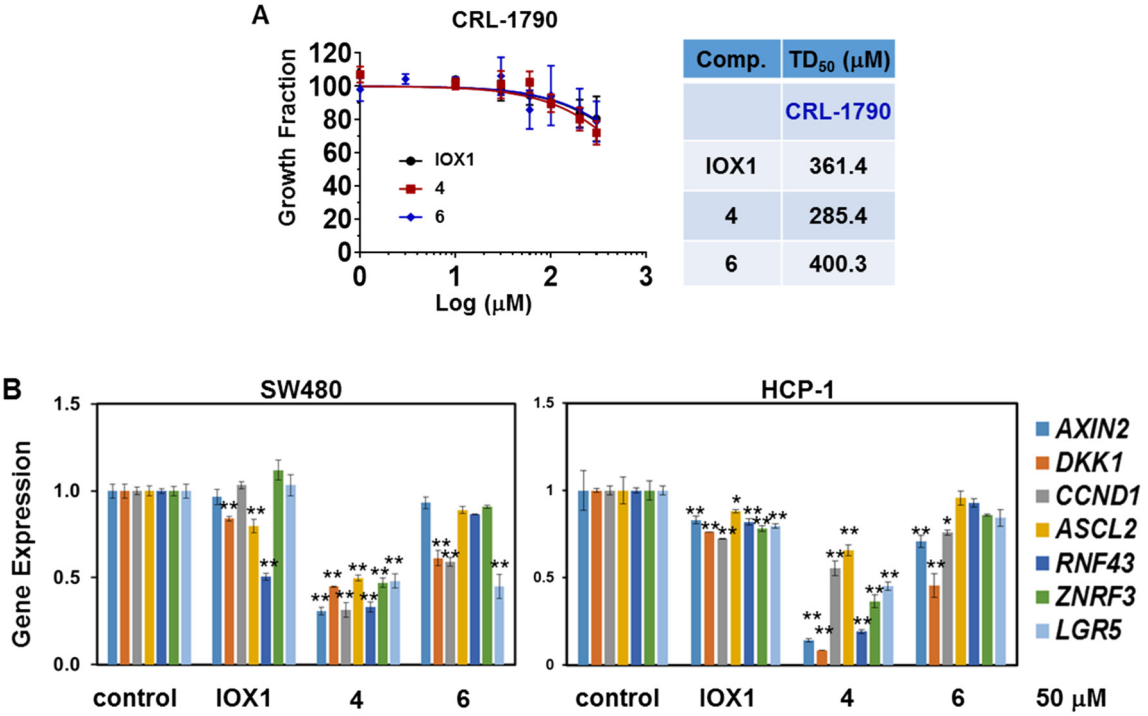

Comp.	TD_{50} (μM)
	CRL-1790
IOX1	361.4
4	285.4
6	400.3

Fig. 4 IOX1-PROTAC suppresses Wnt target gene expression in CRC cells. (A) IOX1-PROTACs had little effect in suppressing the proliferation of CRL-1790 cells. The cells were treated with IOX1-PROTACs as indicated. CCK8 assay was performed 48 h post drug treatment. The TD_{50} values are listed in the table. (B) IOX1-PROTACs inhibited Wnt target gene expression in CRC cells. SW480 cells and HCP-1 were treated with compounds **4** or **6** as indicated for 16 hours. Data represent mean ± SD. $^{**}P < 0.01$; unpaired two-tailed Student's *t*-test.

CSC signature genes, such as *ASCL2*, *RNF43*, *ZNRF3* and *LGR5*, was also strongly inhibited by the two PROTACs (Fig. 4B) in both SW480 and HCP-1. Notably, compound **4** showed a more dramatic inhibitory effect of these Wnt target genes' expression compared to IOX1, demonstrating the superiority to the parental compound.

Clonogenic assay

Clonogenic assay is an effective *in vitro* assay to determine whether compounds can inhibit growth of cells. Both **4** and **6** potently inhibited the colony formation of SW480 and HCP-1 cells in a dose-dependent manner and displayed advantageous doses as compared to IOX1 (Fig. S6A and B†).

Tumorsphere formation assay

ALDH is a well-characterized marker of CSC-like activity in CRC. Previously, we found that $ALDH^{High}$-CSCs have higher expression of KDM3A and KDM3B as compared to $ALDH^{Low}$-non-CSC populations in CRC cells.[16] To evaluate the inhibitory effect of IOX1-PROTACs on CSC-like behavior, tumor sphere formation assays were adopted. Both **4** and **6** displayed potency in suppressing the self-renewal ability of $ALDH^{high}$-SW480 CSCs with around 5-fold higher potency than IOX1 based on their ED_{50} values (Fig. 5A and B). These molecules also potently inhibited the tumor sphere formation ability of $ALDH^{high}$-HCP-1 CSCs. The ED_{50} values were 0.28 μM and 0.51 μM for **4** and **6**, respectively, approximately 20- to 40-fold improvement compared to IOX1 (10.1 μM) (Fig. 5B). The therapeutic index (TI) values for each compound were calculated by normalizing the TD_{50} values of the CCK8 assay with the ED_{50} values. Compounds **4** and **6** showed 28-fold and 21-fold higher therapeutic index than IOX1, respectively (Fig. 5B). Because both KDM3A and KDM3B are significantly upregulated in $ALDH^{High}$-CSCs as compared with $ALDH^{Low}$-non-CSCs, CSCs are more sensitive to KDM3 inhibition, as found in our previous studies.[16] Furthermore, CSCs only represent a small population in cultured CRC cells, which may explain the low IC_{50} values of IOX-PROTACs for CSC-based assays compared to the assays using the whole population of CRC cells.

In vitro metabolic stability and toxicity assessment

There are multiple factors influencing bioavailability, including not only permeability but also hepatic metabolic stability. Hepatic metabolism of small molecules primarily occurs through the cytochrome P450 (CYP) family of enzymes located in the hepatic endoplasmic reticulum, but non-CYP enzymes, such as phase II glucuronosyltransferases and sulfotransferases, also play a significant role.[43,44] To evaluate overall liver metabolism in humans and rats, compound **4** was incubated in liver S9 fractions from both species. The clearance mechanism of compound **4** through phase II glutathione conjugation, glucuronidation and sulfation reactions was studied using glutathione *S*-transferases

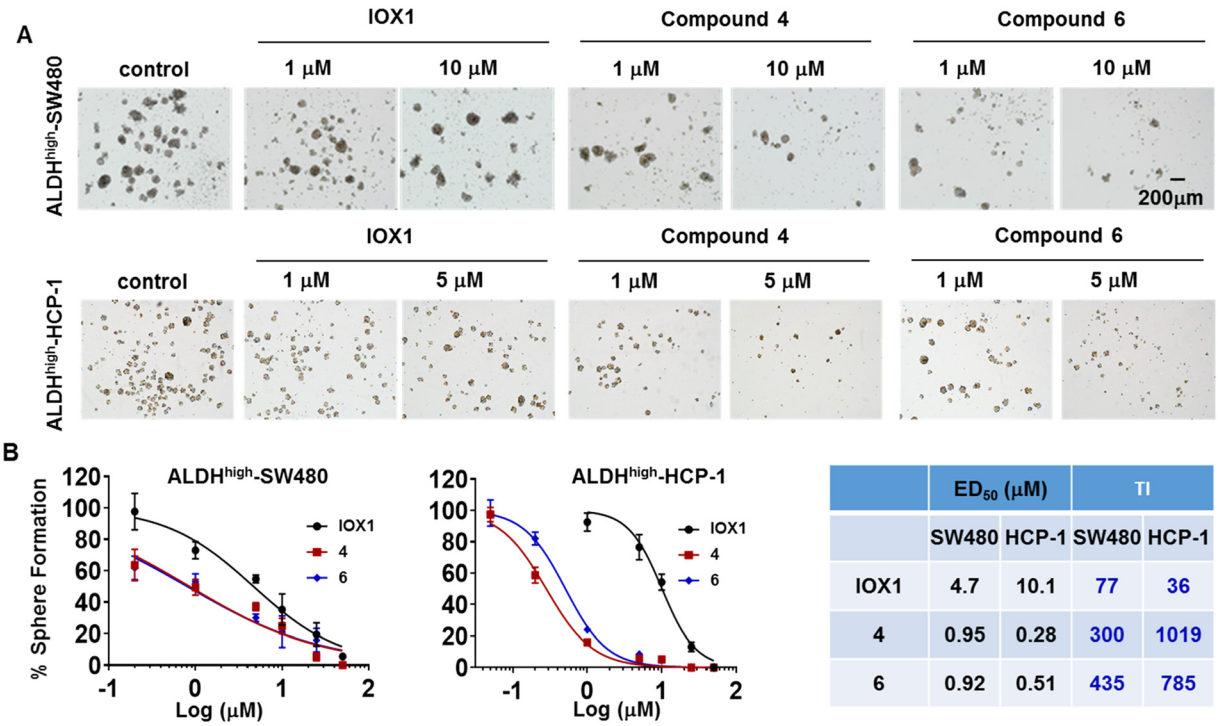

	ED_{50} (μM)		TI	
	SW480	HCP-1	SW480	HCP-1
IOX1	4.7	10.1	77	36
4	0.95	0.28	300	1019
6	0.92	0.51	435	785

Fig. 5 IOX1-PROTAC suppresses self-renewal of CSCs *in vitro*. (A and B) Tumor sphere formation assay showed that the self-renewal ability of CSCs was inhibited by IOX1-PROTACs. The represented images of tumor spheres (A) and dose response curve (B) of treatments in tumor sphere formation assays. The ED_{50} and TI values are listed in the table.

(GSTs), UDP-glucuronosyltransferase (UGT) and sulfotransferase (SULT) enzymes, with the addition of glutathione, uridine-5′-diphospho-α-D-glucuronic acid (UDPGA) and 3′-phosphoadenosine-5′-phosphosulfate (PAPS), respectively.[45] Assuming first-order kinetics, the half-life of compound **4** was calculated to be 16 minutes in human liver S9 fractions and 20 minutes in rat liver S9 fractions (Table 1). This relatively high stability was also observed with the control compound terfenadine, tested in parallel. Furthermore, compound **4** exhibited apparent intrinsic clearance (CL_{int}) values of 41.6 and 34.5 μL min^{-1} mg^{-1} in human and rat liver fractions, respectively (Table 1). According to the CL_{int} classification bands for each species, these values indicate that compound **4** has moderate clearance in both humans and rats.[46,47] This moderate clearance could be ideal for a PROTAC, as it needs to balance sufficient duration for effective protein degradation with timely clearance to avoid prolonged systemic exposure, which could lead to toxicity or off-target effects.

Table 1 Metabolic stability of compound **4** in human and rat liver microsomes

	Human (liver, S9)		Rat (liver, S9)	
Compound	$t_{1/2}$ (min)	CL_{int} (μL min^{-1} mg^{-1})	$t_{1/2}$ (min)	CL_{int} (μL min^{-1} mg^{-1})
Compound **4**	16.7	41.6	20.1	34.5
Clozapine	>120	<5.8	34.0	20.4
Diclofenac	18.5	37.5	101.8	6.8
Imipramine	102.7	22.8	20.3	113.7
Propranolol	>120	<19.3	14.1	164.2
Terfenadine	13.8	167.5	30.6	75.6

hERG-related cardiotoxicity is a critical safety evaluation parameter in early drug discovery campaigns. Compounds that exhibit hERG liability tend to block the inward rectifying voltage-gated K^+ channel (I_{Kr}) in the heart, leading to QT interval prolongation and an increased risk of fatal arrhythmias.[48] Consequently, the hERG inhibitory activity of compound **4** was assessed. Verapamil, an antiarrhythmic drug that selectively blocks the hERG potassium channel, was used as a positive control in the automated patch-clamp assay. The results showed that compound **4** had an IC_{50} value greater than 30 μM, indicating a low potential for causing hERG-related cardiotoxicity.[49]

In vivo anti-tumor activities

Compound **4** was selected to evaluate the efficacy in suppressing the tumorigenic potential of colorectal CSCs *in vivo* based on its highest potency in suppressing expression of colorectal CSC makers and the self-renewal ability of CSCs. $ALDH^{High}$-HCP-1 CSCs were subcutaneously inoculated into the flanks of nude mice. The mice were then treated with IOX1 at 10 mg kg^{-1} or increasing doses of compound **4** at 3 mg kg^{-1}, 10 mg kg^{-1}, 35 mg kg^{-1} (equivalent to the same molar amount of IOX1 at 10 mg kg^{-1}), or control vehicle for 16 days through IP injection. The treatment dose was selected based on Fig. 5 and our previous study, which suggested that the 10 mg kg^{-1} of IOX1 treatment daily can

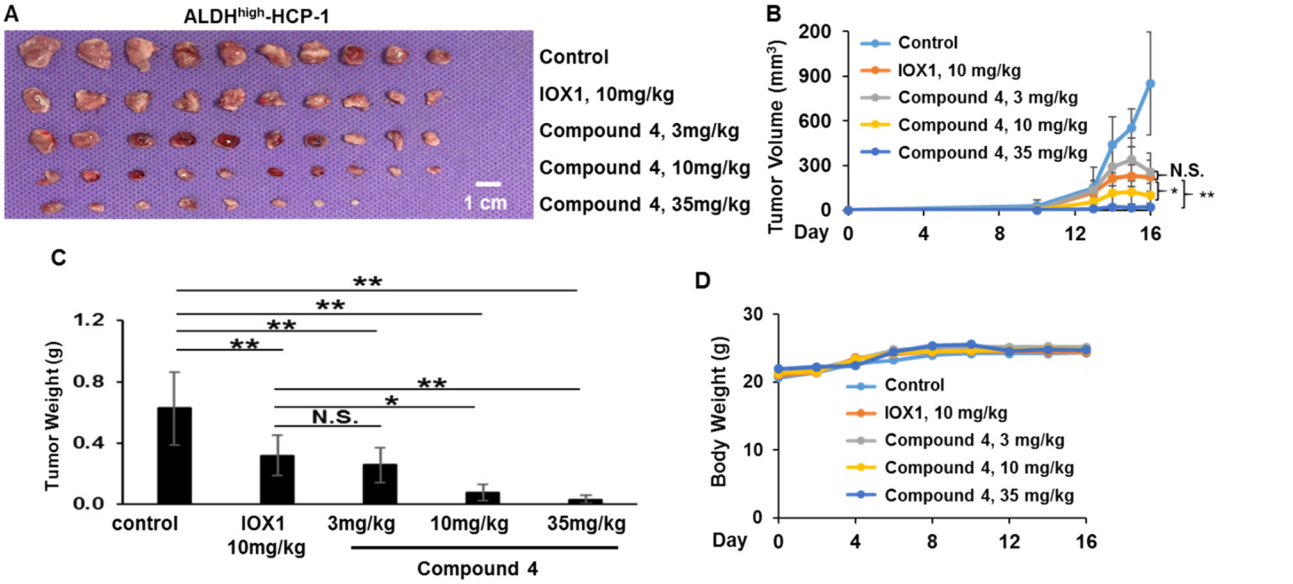

Fig. 6 Compound **4** suppressed the tumorigenic potential of colorectal CSCs. (A and B) Compound **4** significantly inhibited tumorigenic potentials of ALDH^{high}-HCP-1 cells *in vivo*. Data represent mean ± SD (n = 10). *$P < 0.05$ and **$P < 0.01$ by Student's t test. (C) Comparisons of tumor weights at the end of experiments (n = 10). *$P < 0.05$ and **$P < 0.01$ by one-way ANOVA. (D) **4** had little effect on the body weight change of mice.

effectively suppress ALDH^{High}-HCP-1 CSC-derived tumor growth in a similar xenograft mouse model of CRC.[16] As shown in Fig. 6A–C, the CSC-derived tumor growth was significantly inhibited by administration of **4** at all three doses. There was no significant change in the tumor volume nor tumor weight between the IOX1 group and **4** treatment group at 3 mg kg^{-1}, whereas both the tumor volume and weight were significantly decreased in the 10 and 35 mg kg^{-1} treatment groups with at least 10-fold improved potency over IOX1 (Fig. 6A–C). Of note, administration of **4** had little impact on the body weight of mice, suggesting that it is well-tolerated by mice (Fig. 6D).

Immunohistochemical (IHC) staining of the tumor tissues confirmed the PROTAC-induced KDM3A and KDM3B degradation *in vivo* (Fig. 7). The Wnt target gene, *CCND1*, expression was also downregulated upon KDM3 degradation

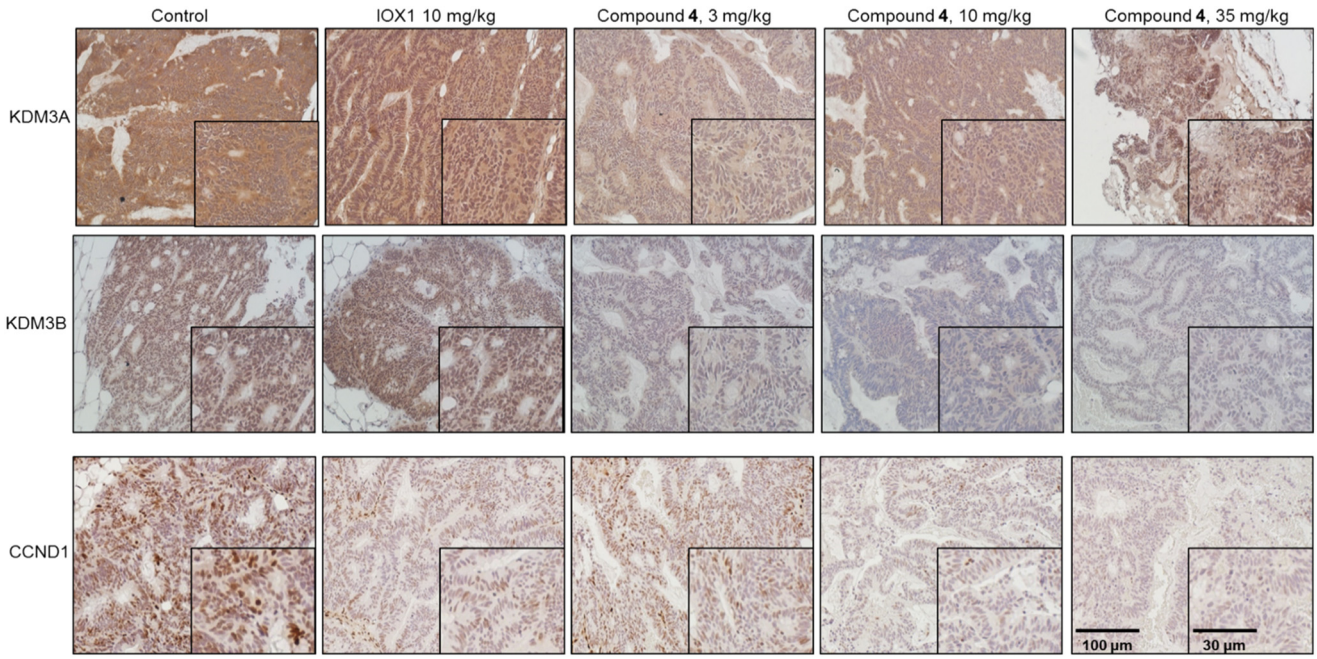

Fig. 7 Administration of compound **4** degrades KDM3 and inhibited Wnt target gene expression in HCP-1 xenografts. Immunostaining of HCP1 xenografts using KDM3A, KDM3B, and CCND1 antibodies.

(Fig. 7). These results suggest that compound **4** has superiority in suppressing Wnt-induced tumorigenesis over IOX1. Interestingly, IHC showed a slight upregulation of KDM3A, but not for KDM3B, in tumors from mice that were treated with 35 mg kg^{-1} of **4** (Fig. 7). This is in line with the *in vitro* "hook effect" of KDM3A identified by western blot assays. Despite the upregulation of KDM3A, the Wnt-induced tumor growth was still drastically reduced in the 35 mg kg^{-1} treatment group, which may be due to the inhibition of the enzymatic activity of KDM3 by the IOX1 functional group in the PROTAC molecules.

Conclusion

Previously, our group demonstrated that KDM3 proteins are overexpressed in colorectal CSCs and control their tumorigenic potential through Wnt/β-catenin signaling. It was also demonstrated that IOX1 can suppress Wnt-induced colorectal tumorigenesis predominantly through enzymatic inhibition of the KDM3 proteins. This formed the basis for utilizing IOX1 to design molecules that target KDM3 proteins with high selectivity and potency, particularly for degrading these proteins using PROTAC technology. In this work, we optimized the linker length through a valid structure–activity relationship (SAR) strategy for a structure-based PROTAC design and developed two PROTACs that have higher selectivity towards KDM3 proteins over KDM4 proteins compared to IOX1. Both PROTACs had higher potency than IOX1, with one (compound **4**) demonstrating up to 35-fold more potency *in vitro* and 10-fold potency *in vivo* than IOX1. Collectively, our investigation suggests that optimization of IOX1-based PROTACs may provide a promising strategy to develop molecules that can effectively suppress oncogenic Wnt signaling to eliminate colorectal CSCs through selective degradation of KDM3 proteins, which may lead to new therapeutics for the eradication of CRC, a life-threatening disease without an effective targeted therapeutic strategy at present.

Experimental

Chemical syntheses

All non-aqueous reactions were carried out under a pre-dried nitrogen gas atmosphere. All solvents and reagents were purchased from either Combi-Blocks, Sigma-Aldrich, or Enamine LLC, and were used as received without further purification. Melting points (mp) were measured on an MPA100 OptiMelt automated melting point apparatus without correction. Analytical thin-layer chromatography (TLC) analyses were carried out on Analtech Uniplate F254 plates and flash column chromatography (FCC) was performed using silica gel (230–400 mesh, Merck). ^{1}H (400 MHz) and ^{13}C (100 MHz) nuclear magnetic resonance (NMR) spectra were recorded on a Bruker Ultrashield 400 Plus spectrometer. Chemical shifts were expressed in δ units (ppm), using TMS as an internal standard, and J values were reported in hertz (Hz). Mass spectra were obtained on an Applied BioSystems 3200 Q trap with a turbo V source for Turbolon Spray. Analytical reversed-phase high performance liquid chromatography (HPLC) was performed on a Varian ProStar 210 system using an Agilent Microsorb-MV 100-5 C18 column (250 × 4.6 mm). All analyses were conducted at ambient temperature with a flow rate of 0.5 mL min^{-1}. HPLC eluent conditions: acetonitrile/water (with 0.1% trifluoroacetic acid), acetonitrile increased from 30% to 100% in gradient within 15 min of test. The UV detector was set up at 210 nm. The injection volume was 5 μL. The purities of the final compounds were calculated as the percentage peak area of the analyzed compound, and retention time (R_t) was presented in minutes. The purity of all newly synthesized compounds was identified as ≥95%.

Step 1. 8-Hydroxyquinoline-5-carboxylic acid (1 eq.) was added portionwise to a stirring suspension of 60% NaH (2.5 eq.) in dry THF (30 mL) at 0 °C, and the resulting mixture was stirred under an inert atmosphere (N_2) for 30 min. Then methoxymethyl bromide (MOM-Br, 2.5 eq.) dissolved in dry THF (20 mL) was added dropwise, and the suspension was allowed to warm to room temperature under an inert atmosphere (N_2). After 4 h, a solution of LiOH (4.0 eq.) in water was added at 0 °C, and the resulting mixture was stirred at room temperature overnight. The reaction mixture was acidified with glacial acetic acid to pH = 4 and then extracted with dichloromethane (DCM; 5 × 90 mL); the organic phases were collected, dried over anhydrous Na_2SO_4, and filtered, and the solvent was removed under reduced pressure to give the target compound as a white solid.

Step 2. A mixture of 2-(2,6-dioxo-piperidin-3-yl)-4-fluoroisoindoline-1,3-dione (1 eq.), *t*-Boc-*N*-amido-PEG#-amine (1.5 eq.), and DIPEA (2 eq.) in DMF (5 mL) was heated to 90 °C and stirred overnight. Upon completion of the reaction *via* TLC, the reaction mixture was diluted with water and ethyl acetate and the organic layer was retrieved. The organic layer was then washed with brine and then dried with Na_2SO_4. The solvent was removed *in vacuo* and the crude product mixture was separated and purified *via* column chromatography (DCM/MeOH, 40 : 1 with 0.1% NH_4OH).

Step 3. The pomalidomide-PEG-*t*-Boc-*N*-amine compound was dissolved in DCM (2 mL) and stirred for 5 minutes at room temperature. Then trifluoroacetic acid (2 mL) was added and the mixture was stirred until the reaction was complete *via* TLC (2 hours). The solvent was removed *in vacuo* and the resulting crude product was then taken to the next step without further purification. The deprotected crude product was dissolved in pre-dried DMF. Then EDCI, HOBt, triethylamine, and molecular sieves were added, and the solution was stirred in an ice bath for 1 hour. After 1 hour, MOM-protected IOX1 was added to the reaction mixture and was stirred overnight at room temperature. Once complete *via* TLC, the reaction was filtered over Celite, the solvent was removed *in vacuo* and column chromatography was run to separate and purify the product (DCM/MeOH, 30 : 1 with 0.1% NH_4OH). The product was then dissolved in methanol

(1 mL), followed by the addition of HCl solution in 1,4-dioxane (4 M). The mixture was stirred at room temperature overnight and then filtered. The target compound was obtained as a yellow solid.

***N*-(2-(2-((2-(2,6-Dioxopiperidin-3-yl)-1,3-dioxoisoindolin-4-yl)amino)ethoxy)ethyl)-8-hydroxyquinoline-5-carboxamide (1).** Yield 89%. ^{1}H NMR (400 MHz, DMSO-d_6) δ 11.08 (s, 1H), 9.27 (d, J = 8.4 Hz, 1H), 9.02 (d, J = 4.2 Hz, 1H), 8.64 (t, J = 5.3 Hz, 1H), 7.92–7.87 (m, 1H), 7.86 (d, J = 8.2 Hz, 1H), 7.56–7.52 (m, 1H), 7.35 (d, J = 8.0 Hz, 1H), 7.15 (d, J = 8.4 Hz, 1H), 6.99 (d, J = 7.1 Hz, 1H), 6.62 (s, 1H), 5.02 (dd, J = 12.8, 5.3 Hz, 1H), 3.70–3.64 (m, 4H), 3.50–3.46 (m, 4H), 2.93–2.84 (m, 1H), 2.58–2.55 (m, 1H), 2.48–2.44 (d, J = 4.0 Hz, 1H), 2.04–1.96 (m, 1H). ^{13}C NMR (100 MHz, DMSO-d_6) δ 172.76, 170.03, 168.90, 167.22, 166.79, 146.40, 145.88, 136.20, 132.01, 129.54, 129.28, 127.18, 123.77, 123.53, 122.79, 122.28, 117.46, 112.43, 110.63, 109.19, 68.74, 64.89, 48.53, 41.73, 30.96, 22.11, 15.15. HRMS calcd for $C_{27}H_{26}N_5O_7$ [M + H]$^+$: 532.1827. Found: 532.1832.

***N*-(2-(2-(2-((2-(2,6-Dioxopiperidin-3-yl)-1,3-dioxoisoindolin-4-yl)amino)ethoxy)ethoxy)ethyl)-8-hydroxyquinoline-5-carboxamide (2).** Yield 48%. ^{1}H NMR (400 MHz, DMSO-d_6) δ 11.08 (s, 1H), 9.28 (d, J = 8.3 Hz, 1H), 9.02 (d, J = 4.3 Hz, 1H), 8.59 (t, J = 5.0 Hz, 1H), 7.90 (dd, J = 8.2, 4.6 Hz, 1H), 7.86 (d, J = 8.0 Hz, 1H), 7.55 (t, J = 7.8 Hz, 1H), 7.34 (d, J = 8.0 Hz, 1H), 7.09 (d, J = 8.3 Hz, 1H), 7.02 (d, J = 7.0 Hz, 1H), 6.58 (s, 1H), 5.05 (dd, J = 12.9, 5.2 Hz, 1H), 3.64–3.59 (m, 8H), 3.49–3.43 (m, 4H), 2.92–2.83 (m, 1H), 2.59–2.56 (m, 1H), 2.55–2.52 (m, 1H), 2.07–1.98 (m, 1H). ^{13}C NMR (100 MHz, DMSO-d_6) δ 173.26, 170.55, 169.40, 167.72, 167.23, 146.79, 146.43, 136.66, 132.51, 129.93, 127.69, 127.64, 124.34, 123.27, 122.05, 117.83, 112.89, 111.14, 109.68, 70.19, 70.08, 69.33, 60.66, 49.02, 44.08, 42.17, 40.63, 31.45, 22.60. HRMS calcd for $C_{29}H_{29}N_5O_8Na$ [M + Na]$^+$: 598.1908. Found: 598.1879.

***N*-(2-(2-(2-(2-((2-(2,6-Dioxopiperidin-3-yl)-1,3-dioxoisoindolin-4-yl)amino)ethoxy)ethoxy)ethoxy)ethyl)-8-hydroxyquinoline-5-carboxamide (3).** Yield 82%. ^{1}H NMR (400 MHz, DMSO-d_6) δ 11.09 (s, 1H), 9.30 (d, J = 8.4 Hz, 1H), 9.03 (d, J = 4.4 Hz, 1H), 8.63 (d, J = 5.0 Hz, 1H), 7.92 (dd, J = 8.3, 4.7 Hz, 1H), 7.87 (d, J = 8.1 Hz, 1H), 7.57 (t, J = 7.8 Hz, 1H), 7.37 (d, J = 8.0 Hz, 1H), 7.11 (d, J = 8.6 Hz, 1H), 7.03 (d, J = 7.0 Hz, 1H), 6.57 (s, 1H), 5.05 (dd, J = 12.9, 5.2 Hz, 1H), 3.60–3.54 (m, 12H), 3.48–3.43 (m, 4H), 2.91–2.88 (m, 1H), 2.61–2.54 (m, 2H), 2.07–1.99 (m, 1H). ^{13}C NMR (100 MHz, DMSO-d_6) δ 173.26, 170.54, 169.39, 167.74, 167.22, 146.84, 146.34, 136.68, 132.53, 130.45, 130.01, 128.08, 127.91, 127.68, 124.35, 123.30, 117.89, 112.99, 111.14, 109.69, 70.32, 70.26, 70.23, 70.07, 69.34, 69.28, 60.65, 49.03, 42.15, 31.45, 22.61. HRMS calcd for $C_{31}H_{33}N_5O_9Na$ [M + Na]$^+$: 642.2170. Found: 642.2170.

***N*-(14-((2-(2,6-Dioxopiperidin-3-yl)-1,3-dioxoisoindolin-4-yl)amino)-3,6,9,12-tetraoxatetradecyl)-8-hydroxyquinoline-5-carboxamide (4).** Yield 87%. ^{1}H NMR (400 MHz, DMSO-d_6) δ 11.07 (s, 1H), 9.18 (d, J = 8.1 Hz, 1H), 8.99 (d, J = 4.3 Hz, 1H), 8.57 (brs, 1H), 7.85 (d, J = 4.3 Hz, 1H), 7.81 (d, J = 8.1 Hz, 1H), 7.57 (t, J = 7.8 Hz, 1H), 7.27 (d, J = 8.0 Hz, 1H), 7.12 (d, J = 8.6 Hz, 1H), 7.03 (d, J = 7.0 Hz, 1H), 6.58 (brs, 1H), 5.04 (dd, J = 12.8, 5.3 Hz, 1H), 3.71–3.66 (m, 4H), 3.52–3.44 (m, 14H), 2.91–2.84 (m, 1H), 2.59–2.53 (m, 2H), 2.06–1.99 (m, 1H). ^{13}C NMR (100 MHz, DMSO-d_6) δ 172.76, 170.03, 168.91, 167.26, 166.93, 146.38, 136.19, 132.06, 131.55, 131.18, 130.50, 130.44, 130.25, 129.11, 127.04, 123.92, 122.72, 117.42, 110.65, 109.22, 72.15, 70.50, 69.81, 69.77 (×2), 69.57, 68.86, 68.81, 60.17, 48.54, 41.68, 30.96, 22.13. HRMS calcd for $C_{33}H_{37}N_5O_{10}Na$ [M + Na]$^+$: 686.2433. Found: 686.2463.

***N*-(17-((2-(2,6-Dioxopiperidin-3-yl)-1,3-dioxoisoindolin-4-yl)amino)-3,6,9,12,15-pentaoxaheptadecyl)-8-hydroxyquinoline-5-carboxamide (5).** Yield 85%. ^{1}H NMR (400 MHz, DMSO-d_6) δ 11.08 (s, 1H), 9.17 (d, J = 8.3 Hz, 1H), 8.99 (d, J = 4.3 Hz, 1H), 8.57 (brs, 1H), 7.82 (s, 1H), 7.80 (d, J = 8.1 Hz, 1H), 7.57 (t, J = 7.9 Hz, 1H), 7.27 (d, J = 7.8 Hz, 1H), 7.13 (d, J = 8.4 Hz, 1H), 7.03 (d, J = 6.9 Hz, 1H), 6.59 (brs, 1H), 5.05 (dd, J = 12.7, 5.4 Hz, 1H), 3.62–3.58 (m, 6H), 3.55–3.53 (m, 6H), 3.45–3.39 (m, 10H), 2.91–2.83 (m, 1H), 2.61–2.55 (m, 2H), 2.06–1.99 (m, 1H). ^{13}C NMR (100 MHz, DMSO-d_6) δ 172.76, 170.02, 168.91, 167.26, 166.97, 146.39, 136.19, 133.27, 132.06, 129.05, 128.97, 127.02, 126.35, 124.95, 124.74, 123.93, 122.70, 117.43, 110.65, 109.22, 69.80, 69.75 (×6), 69.57, 68.86, 68.82, 64.88, 48.55, 41.69, 30.96, 22.12. HRMS calcd for $C_{35}H_{42}N_5O_{11}$ [M + H]$^+$: 708.2875. Found: 708.2873.

***N*-(20-((2-(2,6-Dioxopiperidin-3-yl)-1,3-dioxoisoindolin-4-yl)amino)-3,6,9,12,15,18-hexaoxaicosyl)-8-hydroxyquinoline-5-carboxamide (6).** Yield 85%. ^{1}H NMR (400 MHz, DMSO-d_6) δ 11.05 (s, 1H), 9.13 (d, J = 7.5 Hz, 1H), 8.97 (d, J = 4.3 Hz, 1H), 8.53 (brs, 1H), 7.82 (s, 1H), 7.80 (d, J = 8.1 Hz, 1H), 7.57 (t, J = 6.8 Hz, 1H), 7.24 (d, J = 7.8 Hz, 1H), 7.13 (d, J = 8.3 Hz, 1H), 7.03 (d, J = 5.9 Hz, 1H), 6.58 (brs, 1H), 5.04 (d, J = 12.4 Hz, 1H), 3.64–3.60 (m, 4H), 3.57–3.54 (m, 10H), 3.52–3.48 (m, 14H), 2.92–2.84 (m, 1H), 2.63–2.52 (m, 2H), 2.07–1.99 (m, 1H). ^{13}C NMR (100 MHz, DMSO-d_6) δ 172.68, 169.94, 168.87, 167.22, 167.00, 146.37, 136.14, 132.03, 130.36, 129.12, 128.85, 128.83, 128.82, 126.92, 125.19, 123.91, 122.60, 117.38, 110.61, 109.22, 69.77, 69.73 (×3), 69.71 (×4), 69.54, 68.84, 68.80, 48.53, 41.68, 30.92, 22.09. HRMS calcd for $C_{37}H_{46}N_5O_{12}$ [M + H]$^+$: 752.3137. Found: 752.3100.

***N*-(23-((2-(2,6-Dioxopiperidin-3-yl)-1,3-dioxoisoindolin-4-yl)amino)-3,6,9,12,15,18,21-heptaoxatricosyl)-8-hydroxyquinoline-5-carboxamide (7).** Yield 79%. ^{1}H NMR (400 MHz, DMSO-d_6) δ 11.06 (s, 1H), 9.06 (d, J = 7.6 Hz, 1H), 8.95 (d, J = 4.3 Hz, 1H), 8.50 (brs, 1H), 7.76 (d, J = 7.7 Hz, 2H), 7.57 (t, J = 7.7 Hz, 1H), 7.19 (d, J = 7.7 Hz, 1H), 7.13 (d, J = 8.3 Hz, 1H), 7.03 (d, J = 6.9 Hz, 1H), 6.59 (brs, 1H), 5.05 (dd, J = 12.4, 4.9 Hz, 1H), 3.62–3.58 (m, 4H), 3.57–3.52 (m, 10H), 3.49–3.47 (m, 18H), 2.92–2.84 (m, 1H), 2.61–2.54 (m, 2H), 2.05–2.01 (m, 1H). ^{13}C NMR (100 MHz, DMSO-d_6) δ 172.73, 169.99, 168.90, 167.25, 167.16, 147.14, 146.40, 136.18, 132.50, 132.06, 129.51, 128.71, 128.60, 126.85, 123.94, 122.57, 117.41, 110.97, 110.64, 109.23, 69.80, 69.75, 69.74 (×5), 69.72 (×5), 69.57, 68.86, 68.83, 48.55,

41.70, 30.95, 22.12. HRMS calcd for $C_{39}H_{50}N_5O_{13}$ $[M + H]^+$: 796.3400. Found: 796.3372.

Biological assays

Cell lines. The human colorectal cancer cell lines, SW480 and HCP-1, were obtained from ATCC and MD Anderson Cancer Center, respectively, and were maintained in Dulbecco's modified Eagle medium (DMEM) supplemented with 10% fetal bovine serum (FBS) and 1% pen–strep (Gibco, USA). The normal human colon tissue cell line, CRL-1790, and normal human lung fibroblast cell line, MRC-5, were obtained from ATCC and were maintained in Eagle's minimum essential medium (EMEM) supplemented with 10% FBS and 1% pen–strep. The 293T-TCF-Luc cell line was generated by co-transfecting the pGreenFire1-TCF/LEF (EF1α-puro) lentivector and pPACK-H1 lentiviral packaging plasmid mix into 293T cells to produce the viral particles, transducing the said particles into 293T cells and then selecting the 293T-TCF-Luc cells by treatment with puromycin (1 mg mL^{-1}) for 4 days. All cell lines were tested to be free of mycoplasma contamination and were cultured by incubation at 37 °C in a humidified incubator supplied with 5% CO_2.

Western blotting. Cells were plated in 6-well or 12-well plates and treated with compounds for the specified duration. The total cell lysate was collected at the end of treatment period and the total protein concentration was measured. The lysates were separated using SDS-PAGE and then the proteins were transferred to a PVDF membrane using a semi-dry transfer protocol (Trans-Blot Turbo Transfer System, Bio-Rad). The membranes were incubated with 5% milk (Blotting Grade Blocker, Bio-Rad) for 1 hour. The blots were then incubated overnight at 4 °C with the indicated primary antibodies diluted in 1% milk followed by incubation with the secondary antibody for 1 h at room temperature. All washing steps were performed using Tris-buffered saline with 1% Tween 20 (TBST). The primary antibodies used in this study were: anti-KDM3A (Bethyl, #A301-539A), anti-KDM3B (Bethyl; #A300883A), anti-KDM4A (Bethyl; #A300-861A), anti-KDM4B (Bethyl; #A301-478A), anti-KDM4C (Bethyl; #A300-885A) and anti-α-tubulin (Sigma Aldrich; #T9026).

RT-qPCR. Cells were plated in 6-well plates and treated with the compounds for the specified duration. The total RNA was collected using the NucleoSpin RNA Plus isolation kit (Macherey-Nagel). 1 μg of RNA from each sample was used to synthesize cDNA using the M-MuLV reverse transcriptase kit from New England BioLabs (NEB) and random hexamer primer (ThermoFisher). The cDNA was subjected to qPCR using the SyBRGreen Supermix (Bio-Rad) and primers for the indicated genes. The relative mRNA expression was determined for the indicated genes using the $2^{\Delta\Delta ct}$ method with tubulin expression serving as the internal control. The primers used for the qPCR are listed in Table S1.†

Luciferase assay. 293T-TCF-Luc cells were plated in 12-well plates at 100 000 cells per well density and were treated with the compounds upon attachment to the plate. The Wnt pathway was activated in the cells by treating with 20 mM lithium chloride 4 h post-treatment with the compounds. The cell lysates were collected 16 hours post-treatment with the compounds and the luciferase activity of the total cell lysate was measured using the Bright-Glo luciferase assay system (Promega). For each lysate, the obtained activity was normalized against the total protein concentration.

Sphere formation assay. SW480 and HCP-1 cells were detached from culture plates using 1× trypsin–EDTA (Gibco, USA) and the resulting cell suspensions were passed through 40 μm cell strainers to prepare single-cell suspensions. The $ALDH^{High}$-cells were sorted by staining the cells with the ALDEFLUOR kit (Stemcell) and then running them through the flow cytometer (FACSAria II, BD) using DEAB-treated ALDEFLOUR-stained cells as negative controls. The $ALDH^{High}$ cells were plated in 24-well ultra-low attachment plates at 1000 cells per well density using the serum-free MEBM (Lonza) supplemented with 2% B27 (Gibco), 20 ng mL^{-1} EGF (R&D Systems), 10 ng mL^{-1} FGF (R&D Systems), 4 mg mL^{-1} gentamicin (Invitrogen), 1 ng mL^{-1} hydrocortisone (Sigma-Aldrich), 5 μg mL^{-1} insulin and 100 μM β-mercaptoethanol (Sigma-Aldrich). The cells were treated with the compounds 1 hour after plating. The medium was replenished 1 week later, and the spheres were observed under the microscope 2 weeks post-treatment. The spheres larger than 40 μm were counted to determine the ED_{50}.

CCK-8 based toxicity assay. CRL-1970 cells were plated into 96-well plates at a density of 3×10^3 cells per well and treated with the compounds. The viability of the cells was determined 48 hours post-treatment using the CCK-8 kit (MedChemExpress) and measuring the OD at 450 nm using a microplate reader (Clariostar, BMG Labtech).

Clonogenic assay. SW480 and HCP-1 cells were plated in 12-well plates at 500 cells per well density. Upon attachment to the plate, the cells were treated with the compounds. Fresh media were replenished every 3 days for 2 weeks and then the cells were stained with 0.5% crystal violet. The plates were imaged with a camera and the data were analyzed using ImageJ to determine the ED_{50}.

Hepatic metabolism S9 fraction incubation. 0.1 μM of compound **4** or reference compounds were tested in human liver S9 plus 1 mM glutathione, UDPGA, and PAPS cofactors or rat liver S9 plus 1 mM glutathione, UDPGA, and PAPS cofactors, respectively.[50] At time 0, 15, 30, 45, and 60 min of incubation at 37 °C, the concentration of each compound was determined using HPLC-MS/MS. After the experiment, the metabolic stability, expressed as the percentage of the remaining parent compound, was calculated by comparing the peak area of the compound at the time point relative to that at time 0. The half-life ($t_{1/2}$) was estimated from the slope of the initial linear range of the logarithmic curve of the remaining compound (%) *versus* time, assuming the first-order

kinetics. The apparent intrinsic clearance (CL_{int}, in μL min^{-1} mg^{-1}) was calculated according to the formula: $CL_{int} = 0.693/t_{1/2} \times$ (mg protein per μL or million cells per μL or pmol CYP isozyme per μL).

hERG activity. CHO-K1 cells expressing hERG were plated at least 24 h prior to the experiment and maintained at 37 °C under 5% CO_2. After the whole cell configuration was achieved, the cell was held at −80 mV. A 500 ms pulse to −40 mV was delivered to measure the leak current, which was subtracted from the hERG current on-line. The cell was depolarized to +40 mV for 500 ms and then to −80 mV over a 100 ms ramp to elicit the hERG tail current. This paradigm was delivered once every 8 s to monitor the current amplitude. The parameters measured were the maximum tail current evoked on stepping to 40 mV and ramping back to −80 mV from the test pulse. All data were filtered for seal quality, seal drop, and current amplitude. The peak current amplitude was calculated before and after compound addition and the amount of block was assessed by dividing the test compound current amplitude by the control current amplitude. Control data are the mean hERG current amplitude collected 15 seconds at the end of the control period; test compound data are the mean hERG current amplitude collected 15 seconds at the end of test concentration application for each concentration. All compounds were tested in the presence of 0.1% Pluronic F-68 non-ionic surfactant and at approximately room temperature.

***In vivo* tumor growth.** Twenty-five (25) NSG mice were randomized into five (5) groups ($n = 5$). $ALDH^{High}$ HCP-1 cells sorted by FACS were suspended into Matrigel and 2500 cells injected subcutaneously in both the right and the left flanks. Compound **4** and IOX1 were dissolved in a vehicle composed of PBS and Kolliphor EL (Sigma-Aldrich). Treatment groups received either compound **4** at 3 mg kg^{-1}, 10 mg kg^{-1} or 35 mg kg^{-1} dose or IOX1 at 10 mg kg^{-1} dose administered intraperitoneally while the control group received the vehicle. The body weights were measured every other day and the tumor volumes were measured on days 9, 13, 14, 15 and 16. At the end of the treatment period, the mice were sacrificed and the tumors were collected for further investigation. All animal procedures were performed in accordance with the Guidelines for Care and Use of Laboratory Animals of Virginia Commonwealth University and approved by the Animal Ethics Committee (IACUC AD10002119).

Immunohistochemistry (IHC). The paraffin-embedded cross-sections of the collected tumors were deparaffinized using xylene and alcohol–xylene solution, followed by hydrating the slides in alcohol–water mixtures. Antigen unmasking was performed, and endogenous peroxidase activity was blocked using BLOXALL solution (Vector). The slides were incubated with 10% blocking serum (goat serum in PBS) for 1 hour and then incubated overnight with the indicated primary antibodies at 4 °C in a humidified chamber. The slides were then incubated with biotinylated secondary antibodies for 30 minutes at room temperature followed by staining with the Vectastain Elite ABC kit. The slides were counterstained with hematoxylin. Finally, slides were dried and imaged under the microscope. The antibodies used for IHC were: anti-KDM3A (Abcam, #ab106456), anti-KDM3B (Bethyl, A300-883A) and CCND1 (Abcam, #ab134175).

Abbreviations used

ASCL2	Achaete-scute family BHLH transcription factor 2
ALDH	Aldehyde dehydrogenase
ATCC	American type culture collection
AXIN2	Axis inhibition protein 2
CCK8	Cell counting kit 8
CCND1	Cyclin D1
CSC	Cancer stem cell
CRBN	Cereblon
CRC	Colorectal cancer
DEAB	*N*,*N*-Diethylaminobenzaldehyde
DIPEA	*N*,*N*-Diisopropylethylamine
DKK1	Dickkopf-1
DMF	Dimethylformamide
DMEM	Dulbecco's modified Eagle medium
DMSO	Dimethyl sulfoxide
EDCI	1-Ethyl-3-(3-dimethylaminopropyl)carbodiimide
ED_{50}	Dose effective in 50% of test subjects
EGF	Epidermal growth factor
FACS	Fluorescence activated cell sorting
FBS	Fetal serum albumin
FCC	Flash column chromatography
FGF	Fibroblast growth factor
GSK3	Glycogen synthase kinase 3
HOBt	Hydroxybenzotriazole
HPLC	High performance liquid chromatography
HRMS	High-resolution mass spectrometry
IHC	Immunohistochemistry
KDM3	Histone lysine demethylase 3
KDM4	Histone lysine demethylase 4
LGR5	Leucine rich repeat containing G protein coupled receptor 5
MEBM	Mammary epithelial cell basal medium
MOM	Methoxymethyl
NMR	Nuclear magnetic resonance
PBS	Phosphate buffered saline
PEG	Polyethylene glycol
PROTAC	Proteolysis targeting chimera
PVDF	Polyvinylidene difluoride
qPCR	Quantitative polymerase chain reaction
RNF43	Ring finger protein 43
RT-qPCR	Reverse transcription quantitative polymerase chain reaction
SDS-PAGE	Sodium dodecyl sulfate polyacrylamide gel electrophoresis
THF	Tetrahydrofuran
TLC	Thin layer chromatography
TMS	Tetramethylsilane
ZNRF3	Zinc and ring finger 3

Data availability

The authors confirm that the data supporting the findings of this study are available within the article and its ESI.†

Author contributions

The study was conceived and designed by J. L. and Y. Z. J. L. and Y. Z. developed the methodology. S. U. Z., P. P. P., H. M., and R. G. H. acquired data. S. U. Z., P. P. P., H. M., and R. G. H. analyzed and interpreted the data. The manuscript was written by S. U. Z. and P. P. P. with input from J. L. and Y. Z. J. L. and Y. Z. supervised the study.

Conflicts of interest

There are no conflicts to declare.

Acknowledgements

This work is partially supported by an NIH/NIDCR grants (R03DE026822, R21DE033842, and R01DE033712) to J. L., NIH/NCATS grant (sub-award of KL2TR002648 from NIH/NCATS to VCU's CTSA) to J. L., VCU Presidential Research Quest Fund (J. L. and Y. Z.), and VCU Breakthroughs Fund (J. L.).

References

1 H. Sung, J. Ferlay, R. L. Siegel, M. Laversanne, I. Soerjomataram, A. Jemal and F. Bray, *Ca-Cancer J. Clin.*, 2021, **71**, 209–249.
2 P. Rawla, T. Sunkara and A. Barsouk, *Przegl. Gastroenterol.*, 2019, **14**, 89–103.
3 F. A. Haggar and R. P. Boushey, *Clin. Colon Rectal Surg.*, 2009, **22**, 191–197.
4 E. R. Fearon, *Annu. Rev. Phytopathol.*, 2011, **6**, 479–507.
5 The Cancer Genome Atlas Network, *Nature*, 2012, **487**, 330–337.
6 M. Bienz and H. Clevers, *Cell*, 2000, **103**, 311–320.
7 R. Jackstadt, M. C. Hodder and O. J. Sansom, *Annu. Rev. Cancer Biol.*, 2020, **4**, 177–196.
8 F. de Sousa e Melo, S. Colak, J. Buikhuisen, J. Koster, K. Cameron, J. H. de Jong, J. B. Tuynman, P. R. Prasetyanti, E. Fessler, S. P. van den Bergh, H. Rodermond, E. Dekker, C. M. van der Loos, S. T. Pals, M. J. van de Vijver, R. Versteeg, D. J. Richel, L. Vermeulen and J. P. Medema, *Cell Stem Cell*, 2011, **9**, 476–485.
9 A. G. Schepers, H. J. Snippert, D. E. Stange, M. van den Born, J. H. van Es, M. van de Wetering and H. Clevers, *Science*, 2012, **337**, 730–735.
10 F. de Sousa e Melo, A. V. Kurtova, J. M. Harnoss, N. Kljavin, J. D. Hoeck, J. Hung, J. E. Anderson, E. E. Storm, Z. Modrusan, H. Koeppen, G. J. P. Dijkgraaf, R. Piskol and F. J. de Sauvage, *Nature*, 2017, **543**, 676–680.
11 N. Takahashi, K. Yamaguchi, T. Ikenoue, T. Fujii and Y. Furukawa, *PLoS One*, 2014, **9**, e86582.
12 M. Shimokawa, Y. Ohta, S. Nishikori, M. Matano, A. Takano, M. Fujii, S. Date, S. Sugimoto, T. Kanai and T. Sato, *Nature*, 2017, **545**, 187–192.
13 L. E. Dow, K. P. O'Rourke, J. Simon, D. F. Tschaharganeh, J. H. van Es, H. Clevers and S. W. Lowe, *Cell*, 2015, **161**, 1539–1552.
14 M. Sawa, M. Masuda and T. Yamada, *Expert Opin. Ther. Targets*, 2016, **20**, 419–429.
15 J. Li, B. Yu, P. Deng, Y. Cheng, Y. Yu, K. Kevork, S. Ramadoss, X. Ding, X. Li and C.-Y. Wang, *Nat. Commun.*, 2017, **8**, 15146.
16 R. G. Hoyle, H. Wang, Y. Cen, Y. Zhang and J. Li, *Mol. Cancer Ther.*, 2021, **20**, 191–202.
17 R. Schiller, G. Scozzafava, A. Tumber, J. R. Wickens, J. T. Bush, G. Rai, C. Lejeune, H. Choi, T.-L. Yeh, M. C. Chan, B. T. Mott, J. S. O. McCullagh, D. J. Maloney, C. J. Schofield and A. Kawamura, *ChemMedChem*, 2014, **9**, 566–571.
18 M. Békés, D. R. Langley and C. M. Crews, *Nat. Rev. Drug Discovery*, 2022, **21**, 181–200.
19 X. Wang, Z.-L. Qin, N. Li, M.-Q. Jia, Q.-G. Liu, Y.-R. Bai, J. Song, S. Yuan and S.-Y. Zhang, *Eur. J. Med. Chem.*, 2024, **267**, 116166.
20 A. Mares, A. H. Miah, I. E. D. Smith, M. Rackham, A. R. Thawani, J. Cryan, P. A. Haile, B. J. Votta, A. M. Beal, C. Capriotti, M. A. Reilly, D. T. Fisher, N. Zinn, M. Bantscheff, T. T. MacDonald, A. Vossenkamper, P. Dace, I. Churcher, A. B. Benowitz, G. Watt, J. Denyer, P. Scott-Stevens and J. D. Harling, *Commun. Biol.*, 2020, **3**, 1–13.
21 B. E. Smith, S. L. Wang, S. Jaime-Figueroa, A. Harbin, J. Wang, B. D. Hamman and C. M. Crews, *Nat. Commun.*, 2019, **10**, 131.
22 D. P. Bondeson, B. E. Smith, G. M. Burslem, A. D. Buhimschi, J. Hines, S. Jaime-Figueroa, J. Wang, B. D. Hamman, A. Ishchenko and C. M. Crews, *Cell Chem. Biol.*, 2018, **25**, 78–87.e5.
23 C. Donoghue, M. Cubillos-Rojas, N. Gutierrez-Prat, C. Sanchez-Zarzalejo, X. Verdaguer, A. Riera and A. R. Nebreda, *Eur. J. Med. Chem.*, 2020, **201**, 112451.
24 S.-L. Paiva and C. M. Crews, *Curr. Opin. Chem. Biol.*, 2019, **50**, 111–119.
25 S.-M. Qi, J. Dong, Z.-Y. Xu, X.-D. Cheng, W.-D. Zhang and J.-J. Qin, *Front. Pharmacol.*, 2021, **12**, 692574.
26 P. M. Cromm and C. M. Crews, *Cell Chem. Biol.*, 2017, **24**, 1181–1190.
27 K. Cyrus, M. Wehenkel, E.-Y. Choi, H.-J. Han, H. Lee, H. Swanson and K.-B. Kim, *Mol. BioSyst.*, 2011, **7**, 359–364.
28 R. I. Troup, C. Fallan and M. G. J. Baud, *Explor. Targeted Anti-Tumor Ther.*, 2020, **1**, 273–312.
29 M. Tanaka, J. M. Roberts, H.-S. Seo, A. Souza, J. Paulk, T. G. Scott, S. L. DeAngelo, S. Dhe-Paganon and J. E. Bradner, *Nat. Chem. Biol.*, 2016, **12**, 1089–1096.
30 M. S. Gadd, A. Testa, X. Lucas, K.-H. Chan, W. Chen, D. J. Lamont, M. Zengerle and A. Ciulli, *Nat. Chem. Biol.*, 2017, **13**, 514–521.
31 G. Jones, P. Willett, R. C. Glen, A. R. Leach and R. Taylor, *J. Mol. Biol.*, 1997, **267**, 727–748.

32 M. Vollmar, C. Johansson, C. Gileadi, S. Goubin, A. Szykowska, T. Krojer, L. Crawley, F. von Delft, C. H. Arrowsmith, C. Bountra, A. Edwards and U. Oppermann, Crystal structure of JmjC domain of human histone 3 Lysine-specific demethylase 3B (KDM3B), *PDB crystal structure*, 2013, DOI: **10.2210/pdb4C8D/pdb**.
33 R. P. Nowak, S. L. DeAngelo, D. Buckley, Z. He, K. A. Donovan, J. An, N. Safaee, M. P. Jedrychowski, C. M. Ponthier, M. Ishoey, T. Zhang, J. D. Mancias, N. S. Gray, J. E. Bradner and E. S. Fischer, *Nat. Chem. Biol.*, 2018, **14**, 706–714.
34 G. Lu, R. E. Middleton, H. Sun, M. Naniong, C. J. Ott, C. S. Mitsiades, K.-K. Wong, J. E. Bradner and W. G. Kaelin, *Science*, 2014, **343**, 305–309.
35 J. Krönke, N. D. Udeshi, A. Narla, P. Grauman, S. N. Hurst, M. McConkey, T. Svinkina, D. Heckl, E. Comer, X. Li, C. Ciarlo, E. Hartman, N. Munshi, M. Schenone, S. L. Schreiber, S. A. Carr and B. L. Ebert, *Science*, 2014, **343**, 301–305.
36 L. B. Snyder, J. J. Flanagan, Y. Qian, S. M. Gough, M. Andreoli, M. Bookbinder, G. Cadelina, J. Bradley, E. Rousseau, J. Chandler, R. Willard, J. Pizzano, C. M. Crews, A. P. Crew, J. Houston, M. D. Moore, R. Peck and I. Taylor, *Cancer Res.*, 2021, **81**, 44.
37 L. B. Snyder, T. K. Neklesa, X. Chen, H. Dong, C. Ferraro, D. A. Gordon, J. Macaluso, J. Pizzano, J. Wang, R. R. Willard, N. Vitale, R. Peck, M. D. Moore, C. M. Crews, J. Houston, A. P. Crew and I. Taylor, *Cancer Res.*, 2021, **81**, 43.
38 P. P. Chamberlain and B. E. Cathers, *Drug Discovery Today: Technol.*, 2019, **31**, 29–34.
39 M. E. Matyskiela, W. Zhang, H.-W. Man, G. Muller, G. Khambatta, F. Baculi, M. Hickman, L. LeBrun, B. Pagarigan, G. Carmel, C.-C. Lu, G. Lu, M. Riley, Y. Satoh, P. Schafer, T. O. Daniel, J. Carmichael, B. E. Cathers and P. P. Chamberlain, *J. Med. Chem.*, 2018, **61**, 535–542.
40 M. Pettersson and C. M. Crews, *Drug Discovery Today: Technol.*, 2019, **31**, 15–27.
41 X. Li, W. Pu, Q. Zheng, M. Ai, S. Chen and Y. Peng, *Mol. Cancer*, 2022, **21**, 99.
42 S. B. Hatch, C. Yapp, R. C. Montenegro, P. Savitsky, V. Gamble, A. Tumber, G. F. Ruda, V. Bavetsias, O. Fedorov, B. Atrash, F. Raynaud, R. Lanigan, L. Carmichael, K. Tomlin, R. Burke, S. M. Westaway, J. A. Brown, R. K. Prinjha, E. D. Martinez, U. Oppermann, C. J. Schofield, C. Bountra, A. Kawamura, J. Blagg, P. E. Brennan, O. Rossanese and S. Müller, *Epigenet. Chromatin*, 2017, **10**, 9.
43 F. Esteves, J. Rueff and M. Kranendonk, *J. Xenobiot.*, 2021, **11**, 94–114.
44 M. Zhao, J. Ma, M. Li, Y. Zhang, B. Jiang, X. Zhao, C. Huai, L. Shen, N. Zhang, L. He and S. Qin, *Int. J. Mol. Sci.*, 2021, **22**, 12808.
45 L. Di and R. S. Obach, *AAPS J.*, 2015, **17**, 352–357.
46 J. B. Houston, *Biochem. Pharmacol.*, 1994, **47**, 1469–1479.
47 A.-K. Sohlenius-Sternbeck, L. Afzelius, P. Prusis, J. Neelissen, J. Hoogstraate, J. Johansson, E. Floby, A. Bengtsson, O. Gissberg, J. Sternbeck and C. Petersson, *Xenobiotica*, 2010, **40**, 637–649.
48 A. Garrido, A. Lepailleur, S. M. Mignani, P. Dallemagne and C. Rochais, *Eur. J. Med. Chem.*, 2020, **195**, 112290.
49 H. Yu, B. Zou, X. Wang and M. Li, *Acta Pharmacol. Sin.*, 2016, **37**, 111–123.
50 S. J. Richardson, A. Bai, A. A. Kulkarni and M. F. Moghaddam, *Drug Metab. Lett.*, 2016, **10**, 83–90.